Field implementation of low-cost RFID-based crack monitoring using machine learning

Pierredens Fils [a], Shinae Jang[*] and Rinchen Sherpa [b]

Department of Civil and Environmental Engineering, University of Connecticut,
261 Glenbrook Road Unit, 3037 Storrs, CT 06269-3037, United States of America

Abstract. As civil infrastructure continues to age, the extension of service life has become a financially attractive solution due to cost savings on reconstruction projects. Efforts to increase the service life of structures include non-destructive evaluation (NDE) and structural health monitoring (SHM) techniques. Nonetheless, visual inspection is more frequently used due to high equipment cost from other techniques and federal biennial inspection requirement. Recently, low-cost Radio Frequency Identification Devices (RFID) have drawn attention for crack monitoring; however, it was yet to be implemented in the field. This paper presents a crack monitoring algorithm using a developed RFID-based sensing system employing machine learning under temperature variations for field implementation. Two reinforced concrete buildings were used as testbeds: a parking garage, and a residential building with crumbling foundation phenomenon. An Artificial Neural Network (ANN)-based crack monitoring architecture is developed as the machine learning algorithm and the results are compared to a baseline model. The results show promise for field implementation of crack monitoring on building structures.

Keywords: crack detection; crumbling foundation; machine learning; residential building; RFID; structural health monitoring

1. Introduction

Structural Health Monitoring (SHM) is a broad field that encompasses multiple topics including damage detection, model updating, sensor development, cyber physical systems, and others. Civil structures can experience damage over time, such as fatigue, corrosion, crack propagation, and natural disaster damage. In 2017, the American Society of Civil Engineers (ASCE) infrastructure report card rates infrastructure at a D+ on a national scale (ASCE 2017). To improve infrastructure, service life extension of structures can be accomplished through damage detection. In addition, SHM has been relevant to other fields such as marine (Elshafey *et al.* 2010), aerospace (Giurgiutiu and Zagrai 2005), mechanical (Xia and Curtin 2007), automotive (Medeiros *et al.* 2014), and biomechanical (Muller *et al.* 2008), which have applications where structural damage needs to be detected.

---

[*]Corresponding author, Ph.D., P.E. Associate Professor in Residence, E-mail: shinae.jang@uconn.edu
[a] Ph.D. Student, E.I.T., E-mail: pierre.fils@uconn.edu
[b] Undergraduate Student, E-mail: rinchen.sherpa@uconn.edu

Damage detection is the process of comparing two or more structural systems to identify changes to the materials or geometric properties. The damage identification process consists of damage existence, location, type, and severity (Park *et al*. 2003). This process can be executed for a structure on the global or local scale. In global SHM, an undamaged structure's vibration characteristics are compared with those of a damage structure. This is followed by the implementation of an algorithm that would go through the damage identification process. In local SHM, the existence and location of damage in a structure is known prior. Non-destructive evaluation (NDE) techniques, such as acoustic emission testing, eddy current pulsed thermography, and ultrasonic sensing are then used to identify the type and severity of damage. NDE techniques have proven sufficient results for local SHM but are typically expensive in implementation. Therefore, departments of transportation (DOTs) who have budget constraints tend to not use NDE techniques for mandatory maintenance.

Visual inspection is the most used technique for monitoring steel, concrete, and timber bridges by contractors, state, and County DOT's (FHWA 2001). However, there are limitations with this approach. Visual inspections are based on the inspector's expertise and might result in an inconsistent categorization of damage between projects. Additionally, the tracking of damage is limited by the inspector's line of sight and may lead to gaps in the data logs. Therefore, there is a need for a process that allows for asset tracking, while being cost-effective.

Radio-frequency identification (RFID) technology is used for a broad spectrum of applications like asset tracking and inventory analysis. Due to mass production of tags, RFID is relatively low-cost, time-efficient, and independent of inspector experience. RFID can be categorized as an impedance-based damage detection method where smart piezoelectric ceramic material (PZT) is used as a built-in diagnostic system (Park *et al*. 2003, Giurgiutiu and Craig 1997, Raju 1998, Sun *et al*. 1994, Zagra and Giurgiutiu 2001). As such, RFID technology is an NDE that has gained interest over time due to its material testing capabilities.

For testing, RFID has three components: an RFID tag, reader, and interrogator. The RFID reader transmits a signal to a tag in the form of an electromagnetic field. The tag will receive and backscatter the signal to the reader, where the interrogator will determine the electronic product code (EPC) value and a received signal strength indicator (RSSI) value. The EPC value can be considered as the label or name for a specific tag, letting the user know that tag is located nearby. The RSSI value is a measurement of power reflected from the tag, usually determined by distance from the reader and changes in environment where the tag is attached. Therefore, RFID can be applied to crack detection and the monitoring of the state of the crack.

Recently, researchers have leveraged the theoretical understanding of received power to investigate the use for RFID in terms of crack detection using low-cost commercial RFID sensors. Martínez-Castro *et al*. (2017) verified the performance of a new RFID based crack sensor using low-cost commercial RFID in a lab scale experiment for metal structures. Following this, researchers continued the investigation of RFID based cracks sensors on metal structures (Xu *et al*. 2019, 2020, Marindra and Tian 2019, Marindra *et al*. 2018). Bruciati *et al*. (2019) extended this knowledge to cementitious material and verified its performance in a lab scale experiment. In the lab, researchers were able to achieve a controlled environment. However, for field implementation, a methodology to address environmental fluctuations is required.

Variations in the environment are known to influence RSSI. A study conducted by Amajama (2016) found that an increase in temperature correlated to the decrease in signal strength. In civil structures, changes in temperature and material properties cause a nonlinear effect on the data of interest. Methods to address nonlinear effects on data include traditional statistical methods, like

multivariate linear regression and artificial intelligence (AI). From the late 1980s, an increase in research has emerged using artificial intelligence for structural damage detection, notably, artificial neural networks (ANN). ANNs are an effective method because they can adapt to nonlinear effects during neural network training. Researchers developed an auto-associative neural network (AANN) based method that can consider environmental and operational conditions for structural damage detection (Sohn *et al*. 2002). Also, an ANN-based temperature-effect compensation method was presented by (Sepehry *et al*. 2011) for impendence monitoring in bolted joints. These works show viability for monitoring structures experiencing environmental damage.

Concrete foundations are susceptible to damage due to excessive loading, temperature, humidity, and material degradation due to chemical reactions. In Eastern Connecticut, many municipal and residential buildings are impacted by Crumbling Foundations (Holleran 2020). In Connecticut, crumbling foundations involve the deterioration of concrete due to the presence of a pyrrhotite-bearing aggregate (Duchesne and Fournier 2013). In the presence of oxygen and water, pyrrhotite undergoes sulfide oxidation to produce iron oxyhydroxides and sulfuric acid. The resulting sulfuric acid reacts with Portland cement paste phases to create gypsum and ettringite. The formation of these two products causes an increase in volume, which leads to an expansion in the concrete structure and ultimately cracking (Duchesne and Fournier 2013). The formation of said cracks can be observed around 10 to 30 years into the structure's service life (Schaefer and Schaefer 2020). Therefore, low-cost RFID-based crack sensors can be beneficial to monitor such crack propagation.

In this paper, a systematic approach for crack detection using machine learning under environmental fluctuations has been developed and experimentally implemented for two building structures using the low-cost RFID-based sensors. Multivariate Linear Regression (MLR) and Artificial Neural Networks (ANN) have been adopted for predicting crack propagation under environmental variabilities, and their performances have been compared. The testbed structures are a reinforced concrete parking garage building and a residential building with a crumbling foundation in Connecticut. An RFID-based crack sensor has been installed on multiple locations with varying cracks. The crack width, environmental factors, and RFID tags' RSSI have been measured. Using the measured data, the ANN-based crack prediction analysis has been conducted. This research is the first field implementation of the low-cost RFID-based crack sensors on building structures.

2. Theoretical background

This section presents an overview of the theory used to conduct this work. The development of RFID-based crack sensors is explained through the received signal strength indicator (RSSI). The baseline methods including MLR, ANN, and weighted percent error have also been presented for completeness.

2.1 Received signal strength indicator

An RFID-based crack sensor has been developed based on the correlation of crack appearance, to the change in impedance and radiation characteristics (Kalansuriya *et al*. 2013)

$$P_R = \frac{P_T(G_T G_R)}{4\pi}\left(\frac{\lambda}{(4\pi R_T R_R)^2}\right)^2 \sigma \tag{1}$$

where, P_R is the backscatter power in dB, P_T is the transmitted power in dB, G_T is the transmitting antenna gain in dB, G_R is the receiving antenna gain in dB, λ is the signal wavelength in meters, R_T is the distance between the target and the transmitting antenna in meters, R_R is the distance between the target and the receiving antenna in meters, and σ is the targets radar cross section in meters^2.

Using ultra-high frequency (UHF) passive RFID tags as sensing units, the most important measured values for crack detection from a tag, the RSSI, can be obtained

$$RSSI = 10log_{10}\left(\frac{P_R}{1\text{mW}}\right) \tag{2}$$

where RSSI is the received signal strength indicator in dB.

2.2 Multivariate linear regression

To establish a baseline correlation between independent and dependent variables, a multivariate linear regression (MLR) method has been used. MLR is a method used to estimate the size and statistical significance of the relationship between these variables. MLR can be defined as follows

$$\boldsymbol{Y} = \boldsymbol{XB} + \boldsymbol{E} \tag{3}$$

where $\boldsymbol{Y}$ is the response matrix, $\boldsymbol{X}$ is the design matrix, $\boldsymbol{B}$ is the matrix of coefficients, and $\boldsymbol{E}$ is the error matrix (Helwig 2017). Therefore, MLR methods are used for multi-output cases.

2.3 Artificial Neural Network (ANN)

An Artificial Neural Network (ANN) is a computational system designed to mimic the performance of the human brain. The ANN finds patterns in data, which are too complex or too large for typical computational systems, by analyzing past data (Dormehl 2019). The model hyperparameters are parameters that determine how the model is trained and how it is structured. A particular set of hyperparameters can be classified as the architecture of the model. This architecture determines the patterns that will be learned by the model given a set of data. Here, the architecture defines algorithms like the loss function and optimizer, along with structure of the network (Leonel 2019).

To judge the performance of the ANN model, the mean squared error (MSE) metric has been used because of its enhanced ability to handle the multi-output case. The MSE is estimated over the number of samples, n_{samples}, such that

$$MSE(y_i, \hat{y}_i) = \frac{1}{n_{samples}} \sum_{i=0}^{n_{samples}-1} (y_i - \hat{y}_i)^2 \tag{4}$$

where $\hat{y}_i$ is the predicted value of the i-th sample, and y_i is the corresponding true value.

The Loss function is another hyperparameter that serves to compute the quantity that a model should seek to minimize (Keras 2015). When the distribution of the target variable is mostly gaussian, but has some outliers, an acceptable loss function to use is MAE (Brownlee 2018). Therefore, MAE is estimated over n_{samples}

$$MAE(y_i, \hat{y}_i) = \frac{1}{n_{samples}} \sum_{i=0}^{n_{samples}-1} |y_i - \hat{y}_i| \qquad (5)$$

where $\hat{y}_i$ is the predicted value of the i-th sample, and y_i is the corresponding true value.

For the optimizer, Adagrad was used because it is a gradient-based optimizer designed to updates infrequent parameters at a higher rate than frequent parameters (Ruder 2017). This attribute lead makes Adagrad well suited to handle datasets have a sparse nature, which is typically the case in experimental work.

2.4 Model performance validation

The performance of the predicted MLR and ANN models have been compared to the real crack widths obtained via visual inspection. To do this, the analysis consists of a percent error

$$\%Error = \frac{|(Predicted_{Model} - Real_{Data})|}{(Real_{Data})} \times 100 \qquad (6)$$

where, $Predicted_{Model}$ is the predicted crack width for the MLR or ANN model and the $Real_{Data}$ is the crack width collected via visual inspection. However, to account for non-crack values, or cracks of width 0, Eq. (6) is modified as follows

$$\%Error_{weighted} = \frac{|(Predicted_{Model} - Real_{Data})|}{(Real_{Data} + 1)} \times 100 \qquad (7)$$

3. Methodology

In this section, an overview of the methodology is presented. The damage detection process from planning a monitoring site and the crack prediction architecture using ANN are discussed. An overview of the experimental setup has been presented with the components of an RFID-based sensing system and equipment specifications. The information of the two test sites and testing logs have also been discussed.

3.1 Damage detection procedure

The damage detection procedure follows a crack detection flowchart shown in Fig. 1. Site planning involves identifying locations with necessary monitoring points, initializing the necessary sensors, such as RFID tags, and preparing equipment, e.g., reader and data collection tool. Data collection involves capturing screen recordings of continuous data for all testing sets, while also recording the pertinent weather data corresponding to the testing time. The data cleaning phase involves the transformation of recorded data to individual frames and the selection of data points at a uniform sampling rate. The data pre-analysis phase requires statistical metrics to be calculated to create a data frame with statistical metrics and weather information to correspond to the crack width. Finally, the produced data frame is utilized inputs to the ANN Architecture that will be discussed in the next section. This flowchart procedure allows for the integration of prediction models for field testing.
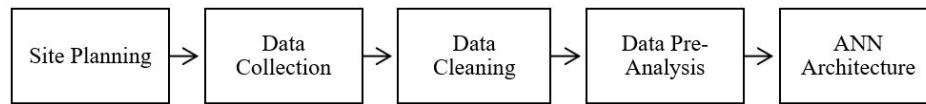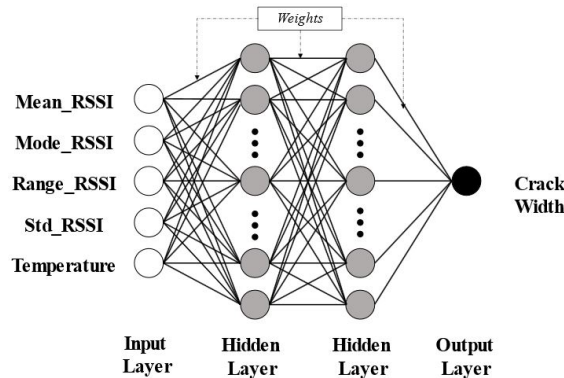
Fig. 1 Crack detection flowchart

Fig. 2 ANN architecture

3.2 ANN-based damage prediction architecture

A base ANN model has been created to aid in the identification of cracks and the quantification of their corresponding widths. The hyperparameters of this model have determined the network structure and the training process. The network structure contains 4 layers as shown in Fig. 2. The input layer has 5 nodes corresponding to the input parameters. The input parameters describe the RFID data series along with the environmental conditions during testing. This has been followed by 2 hidden layers that have 100 nodes each. The nodes in the hidden layer determine the capacity for the model to learn (Dormehl 2019). 100 nodes were selected via experimentation to avoid overfitting of the model to the data. The last layer is the output layer and contains only one node. This node is the crack width prediction given by the ANN model.

The algorithm developed is defined by several steps per epoch shown in Fig. 3. First, the weights, or parameters, of the model are randomly initialized at the beginning to small numbers close to zero. The first row of observations is then inputted into the input layers where each feature corresponds to an input node. Forward-propagation occurs from left to right, where the neurons are activated so that the impact of each neuron's activation is limited by the weights. Propagations occur until a predicted values of crack widths, Y_{pred}, is found. The prediction values are compared to the validation, Y_{val}, and a loss is obtained. Once the loss is obtained, back-propagation, or from right to left, the error is used to update the weights to minimize the loss function. The algorithm then updates the weights and iterates the next batch of input observations. Once the iterations through all batches are complete, the training has successfully gone through one epoch. This process makes use of a batch size of 2 and 100 epochs.

3.3 Experimental setup

The testing equipment includes a handheld reader, RFID tags, Measurement Methods (MMs),
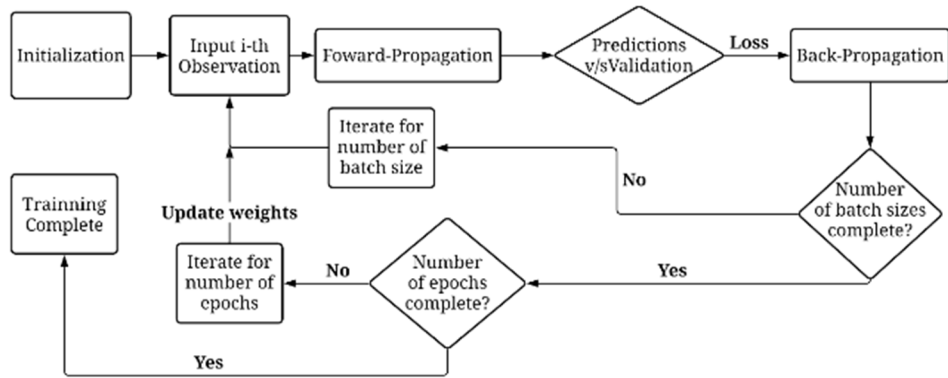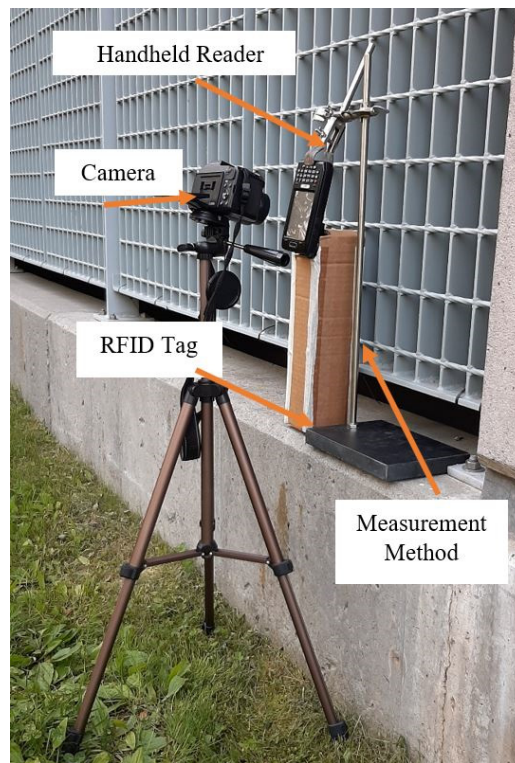
Fig. 3 ANN Procedure
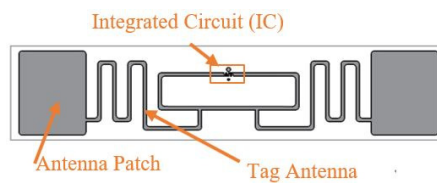

Fig. 4 Experimental setup

Fig. 5 Alien Technology ALN-9662 short inlay tag

and a camera as shown in Fig. 4. The ATID AT870N UHF Handheld Reader with anti-collision technology (ATID 2019) has an operating frequency of CE 865 MHz-868 MHz and FCC 902 MHz-928 MHz and a read range up to 5 meters. For RFID-tags, the Alien Technology ALN-9662 short inlay tag was used. This tag is EPG Gen 2 and ISO/IEC 18000-6C compliant and uses a Higgs 3 EPC Class 1 Gen2 RFID tag integrated circuit (IC). The tag IC is made of a flexible metallic material, which is adhered to a wet inlay (Alien 2014). Due to its commercial availability, the price per tag when purchased in bulk is around $0.10 to $0.20 in terms of purchasing size. A detailed view of the tag can be seen in Fig. 5. The sensor was directly attached on the concrete surfaces with masking tapes without substrate material. As cementitious materials are different than metal surfaces, the RSSI can be readily measurable on the material because of its low relative permittivity.

Additionally, measurement methods (MMs) developed by Fils and Jang (2020) have been used to provide a controlled environment with accurate and consistent results. Researchers accomplished this by creating measurement methods (MMs), which consisted of cardboard enclosures of varying characteristics. The MMs that were most effective at controlling environmental effects on RFID readings have been employed for this paper. These MMs are MM_A1 and MM_A3.2 with dimensions of [length x width x depth]. MM_A1 is a cardboard box construction with dimensions [12 in × 3 in × 3 in] where all four antenna surface areas are connecting. MM_A3.2 is a cardboard box construction with dimensions [12 in × 3.25 in × 2.75 in] where all four antenna surface areas are connecting, and the internal corrugations are exposed (Fils and Jang 2020). All MMs are slightly different but the length, read distance, or interrogation distance have been kept constant in this work.

4. Testbed 1: Reinforced concrete parking garage

4.1 Testbed description

For the first test bed, a precast reinforced concrete (RC) parking garage building at the University of Connecticut (UConn), as seen in Fig. 6, was adopted (Vistols 2020). Built in 1998, this build project encompasses 5 levels and holds 1,035 parking spaces (Unistress 1998). Located in New England, this building has been exposed to high and low temperature extremes. As a result, the exterior walls of the parking garage have various ranges of thermal cracks on concrete covers, which have been regarded as crack variation of the first set of experiment. However, no exposed rebar or other damage have been identified at the testing locations.

The surface cracks, that have been induced by thermal shrinkage on the walls at the foundation level of the building, have been selected for testing because further cracking in-service building is prohibited. In total, four locations have been considered: one undamaged location for control, and three cracked locations with varying crack widths. The crack width and visual representations of these locations are shown in Table 1.

The tests were conducted in accordance with the crack detection flowchart discussed in Section 3.2. The equipment and RFID tags described in section 3.3 have been employed. At each location, the RSSI has been collected for a time span of 60 seconds at a 25 Hz sampling rate. The temperature data at the start of each measurement was collected. The raw data were cleaned deleting the first 5 seconds and the last 5 seconds, and down-sample the middle 49 seconds at a 5 Hz. In total, 160 samples are used for analysis.

Fig. 6 North Campus Parking Garage (Vistols 2020)

Table 1 Damage description

Location	Identification	Crack width (in)	Visual representation
1	No crack (Control)	0.000	
2	Vertical crack	0.020	
3	Vertical crack	0.025	
4	Vertical crack	0.030	

*X mark indicates the location where the left RFID patch was aligned when installed

4.2 Results

4.2.1 Statistical analysis

To provide a comprehensive view of the measure data, various statistical measures were implemented among RSSI, temperature, and crack width. Distributions of the average, mode, standard deviation (StDev), and range of the individual samples were correlated to either
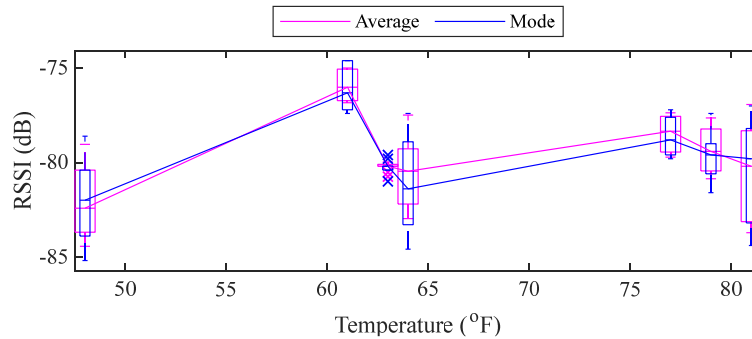
Fig. 7 Average RSSI and mode versus temperature

temperature or crack width. In Fig. 7, the correlation of the average and mode of the RSSI vs temperature is shown. Both the average and mode are in alignment and increased by an average of 2 dB, as the temperature rises from 48°F to 81°F. Overall trend is proportional; however, it shows nonlinear behaviour around 61°F. This brings rise to potential future work to further investigate potential unknown factors. Possible parameters for future work include humidity, dew points, as well as the existence of hidden cracks underneath. To check the robustness of the developed ANN model, the results have been included in the training and test sets.
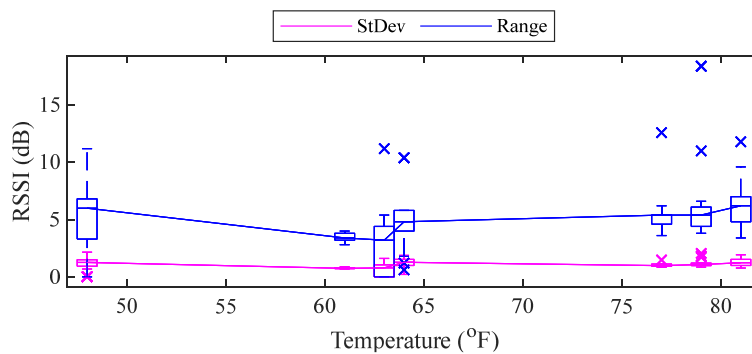
Fig. 8 North garage RSSI standard deviation and range versus temperature
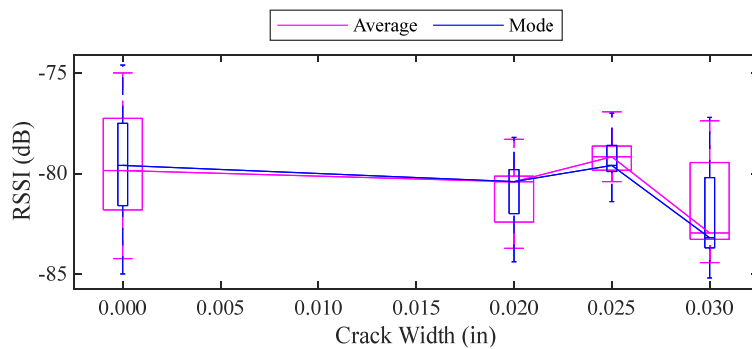

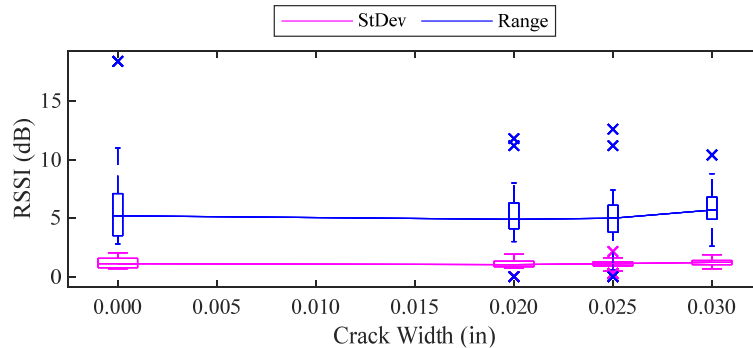Fig. 9 North garage RSSI average and node versus crack width

Fig. 10 North garage RSSI standard deviation and range versus crack width

In Fig. 8, the StDev and range are plotted relative to temperature to illustrate the dispersion properties of the different samples. The StDev is consistent around 1 dB for all temperatures, signifying that temperature did not have a significant influence on the StDev. The range was fluctuating above and beyond 5 dB and experienced significant outliers at higher temperatures.

After the correlation between RSSI vs. temperature was analyzed, the correlation between RSSI and crack width was investigated. In Fig. 9, the average and mode of all samples relative to the crack width is presented. Relative alignment of the average and mode are present along with an average decrease of 2 dB as the crack width increase from 0 to 0.3 inches.

Next, in Fig. 10, the StDev and range of the RSSI relative to crack width is reported. Similar to the correlation between RSSI and the temperature, the StDev was consistent around 1 dB. However, in terms of the range, more outliers are present throughout different widths.

The average and mode describe the correlation of RSSI to temperature or crack width, while StDev and range speak to the stability of testing. A general increase in average and mode RSSI is depicted as the temperature increases, while the standard deviation and range remain stagnant with a few outliers. The mixed behaviour of temperature and crack width, with respect to RSSI descriptive variables, add additional complexity to field testing; leading to the implementation of the damage identification method using ANN.

Using the statistical measures of interest and environmental conditions, a data frame was created. This data frame contained average, mode, standard deviation, and range of the RSSI values along with the temperature and crack width corresponding to the location of damage.

4.2.2 Machine learning-based measures

The ANN for crack detection was created based on Figs. 2 and 3, and its crack prediction performance was validated with experimental data. Among all measured data, 90% of data was used to train and create the ANN for crack prediction. Then, the remaining 10% of data was inputted into ANN, so that it will output the crack quantities. For comparison, an MLR prediction was employed.

In the process of training ANN, the loss function was plotted using a mean absolute error, Eq. (5), and a metric for model performance was used as the mean squared error, Eq. (4)). Fig. 11 shows the training data along with the validation sets. As we train the ANN with more epochs, convergence of the training and validation data is reached. The convergence is an indication that that the model is sufficiently trained. Based on the loss functions and mean square error, the trained ANN shows stable convergence.

(a) Model loss   (b) Model accuracy
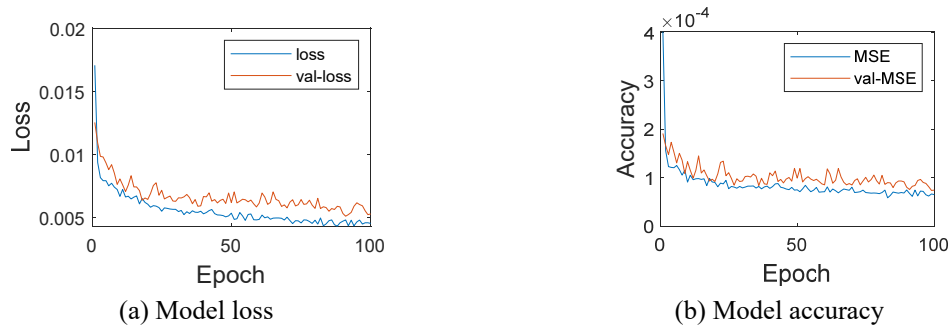
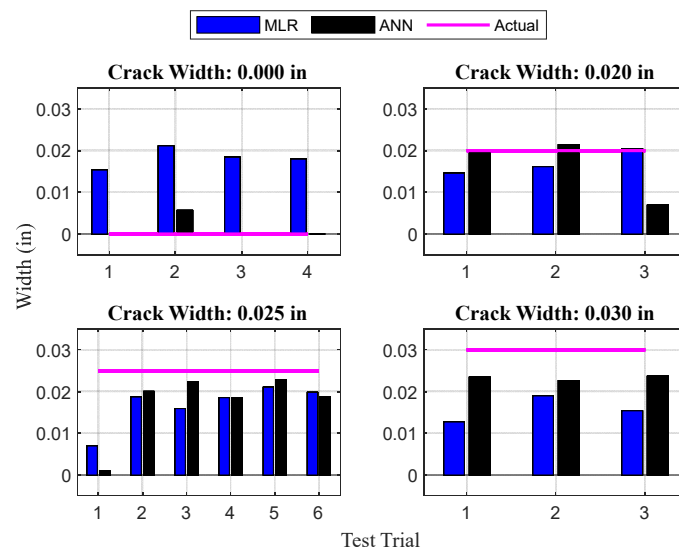Fig. 11 Results for 90% trained ANN model

Fig. 12 Crack width predictions for MLR and ANN

Using the trained ANN, the crack quantities were predicted as shown in Fig. 12. Test trials were randomly chosen and input to ANN. For each trial, the crack prediction using ANN and MLR are shown and is compared with the actual crack quantities. The top left chart of Fig. 12 shows cases where there was no crack present. The ANN outperformed the MLR in these cases. The interconnected layers of the ANN were able to identify additional feature and provided a higher level of prediction flexibility to the ANN. Hence, the ANN model was able to learn the difference between a cracked and non-cracked case. The other cases predicted are 0.020 in, 0.025 in, and 0.030 in, shown in the top right, bottom left, and bottom right respectively. Here we see the ANN predictions are in close alignment to the actual crack widths. Additionally, the ANN performance exceeded that of the MLR.

In addition, the error in the model's crack prediction is calculated as shown in Fig. 13. Considering the 16 test trials, the ANN predicted closer to the true value 12 out of 16, or 75% of the time. The MLR had a 1.07% error with a standard deviation of 0.65% while the ANN had a 0.53% error with a standard deviation of 0.59%. Both methods provided reasonable crack
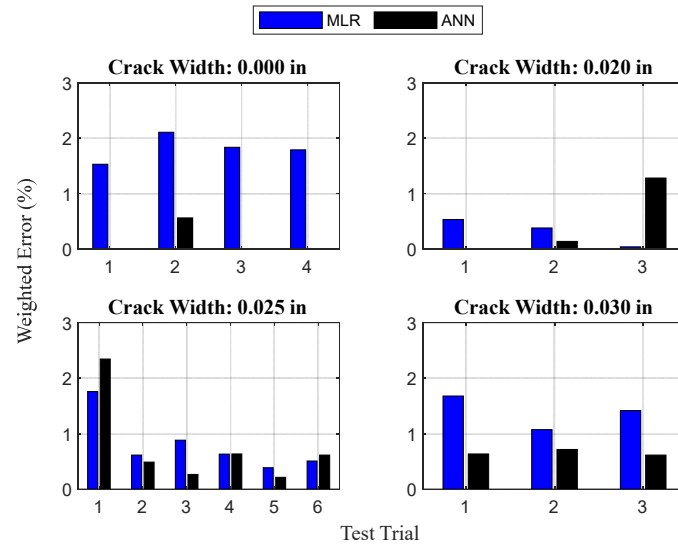
Fig. 13 Error in crack width prediction from the MLR and ANN models

detection performance, however, the ANN predicted the crack widths more accurately than the MLR because of the deep learning capabilities of ANN. During the training of the ANN, the model was able to adapt to nonlinear effects by accounting for the variability in temperature and differentiating a cracked and a non-cracked case as small as 0.01 inches in width.
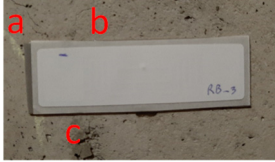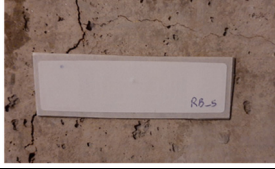
5. Testbed 2: Residential building with crumbling foundation

To investigate the overall nature of the Crumbling foundation cracking and its relative crack sensor sensitivity, a test bed that encompass multiple crack types is ideal. A test bed that also accounts for variables such as temperature, and varying crack widths is needed to accurately classify RFID crack sensor sensitivity.

5.1 Testbed description

A residential building in Coventry CT was identified as a crumbling foundation. Based on a visual examination report (Schaefer and Schaefer (2020), a licensed professional engineer concluded that the visible cracking patterns commonly associated with deleterious pyrrhotite-bearing aggregate are present, with crack widths less than 1.0 mm (0.39 in) that extend less than 20% of any contiguous wall plane. If these cracks surpass widths of 1.0 mm (0.39 in) then a category 3 would be initiated and a critical decision by the owner would need to be made. For crumbling foundations, no effective retrofitting method is known, therefore, the owner should either replace the foundation or vacate the premises. The tracking of the crack widths would be instrumental in determining this critical decision. For accurate crack evaluation, NDE method including X-Ray Fluorescence (XRF), Light Detection and Ranging (LiDar), Ultrasound, Ground Penetrating Radar (GPR) are desired (Gobi and Ashe 2019, Lienert and Lee 2020, Daniel 2020). However, a typical owner has limited access to high-cost high precision technology, and low-cost

Table 2 Damage description

Location		Crack type	Initial crack width (in)	Visual representation with RFID tags
1		Vertical	0.004	
2		Vertical	0.004	
3	A	Intersection of three cracks	0.009	
	B		0.004	
	C		0.009	
4		Vertical	0.016	
5		Vertical	0.004	
6		Horizontal	<0.004*	

*0.004 was the minimum scale of the crack ruler used in the test

crack evaluation can be desired. Therefore, crack monitoring using the RFID-based crack sensors was considered and long-term experiment was conducted.

For a holistic view of the site, an initial visit was made. Through this visit, it was revealed, through owner account, that large cracks existed before purchasing the unit and the nearby residents were dealing with similar issues. In addition, expert investigation concluded the presence of shrinkage cracks ranging from 1-2 mm in the vertical direction, gypsum powder surrounding spider-like cracks on an interior non-load bearing wall, and hair line crack both vertical and horizontal on the surface of an exterior load bearing wall. For testing purposes, Table 2 illustrates 6 damage locations with varying crack type and width that were adopted.

The experiments of this residential building were conducted using the identical procedure as the testbed 1 in accordance with the crack detection flowchart discussed in Fig. 2. The experiments were planned for 1 year; however, actually conducted for 4 months between November 2019 to February 2020. The long-term experiment has stopped because of the COVID-19 pandemic in March of 2020.
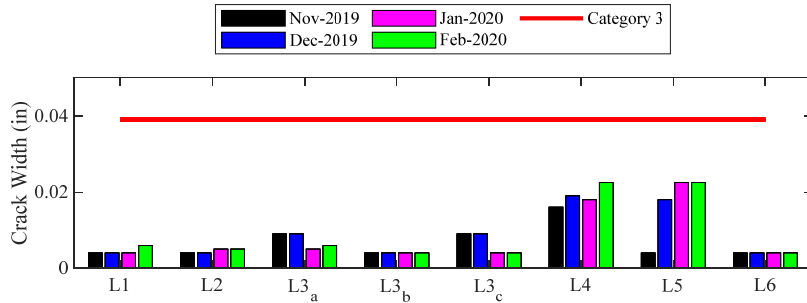
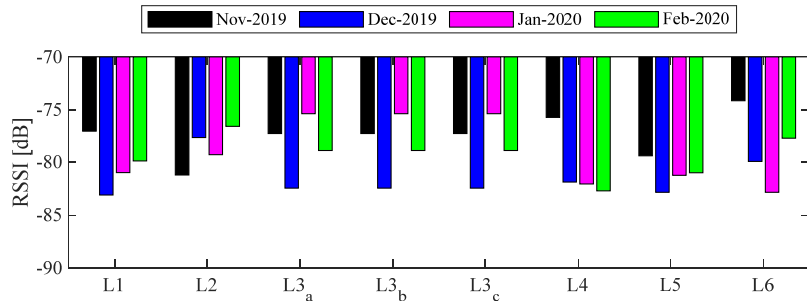Fig. 14 Log of crack width via visual inspection over time

Fig. 15 Log of average RSSI values for damage locations over time

5.2 Results

5.2.1 Visual inspection of cracks

Visual inspection techniques and frequent site visits allowed for an initial analysis of the damage cases. The crack widths for the 6 different damaged locations were monitored as shown in Fig. 14. The threshold that separates a category 2 from a category 3 is denoted by the horizontal red solid line. Testing locations 4 and 5 are approaching the limit and need to be closely monitored. Other locations seem temporarily stable but can experience change in future observations.

5.2.2 RSSI and statistical analysis

Fig. 15 shows the average raw RSSI values computed for six different crack locations on four different tests, with the last two dates having two tests each. For Location 4, the overall crack width increased while the RSSI decreased. Therefore, a direct correlation between the crack width and the RSSI is shown. Overall, an inverse correlation between RSSI and crack width is presented. Location 5 is of particular interest because in Fig. 14, a high relative change in crack width between the November and December tests. Similarly, in Fig. 15, this phenomenon is reflected by the RSSI decreasing from -79 to -83 in dB scale. For locations 1, 2, 3, and 6, the crack width was smaller than 0.01 inches and no clear correlation was found. Past studies concluded that for cracks that are larger than 0.01 inches, a proportional relationship between the RSSI and crack width can be captured (Martínez-Castro *et al*. 2017, Bruciati *et al*. 2019, Sherpa *et al*. 2021).

To provide a comprehensive view of the measure data, various statistical measures were implemented among the RSSI, temperature, and crack width. The distributions of the average,
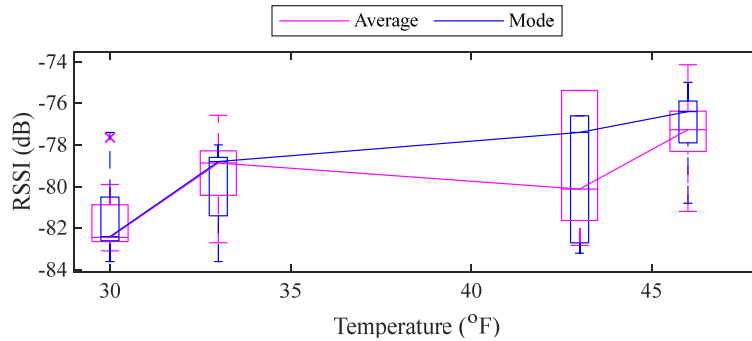
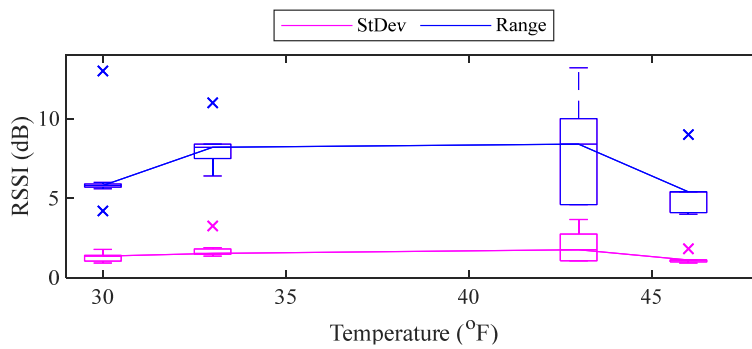Fig. 16 Correlation between average and mode RSSI and under temperature

Fig. 17 Correlation between standard deviation and range RSSI and under temperature

mode, standard deviation, and range of the samples as were correlated either temperature or crack width. Fig. 16 shows the correlation between the average and mode of all samples relative to the temperature. Both measurements are in alignment and increase by an average of 4 dB as the temperature rises from 30°F to 46°F reflecting the early winter season in New England. Overall, the average and mode of the RSSI are proportional to the temperature.

Next, the StDev and range of the RSSI are plotted relative to temperature in Fig. 17. Similar to the results of testbed 1, the StDev remains around 1 dB for all temperatures indicating that
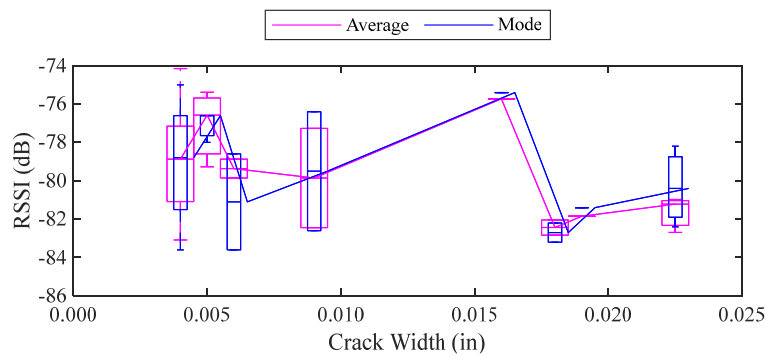

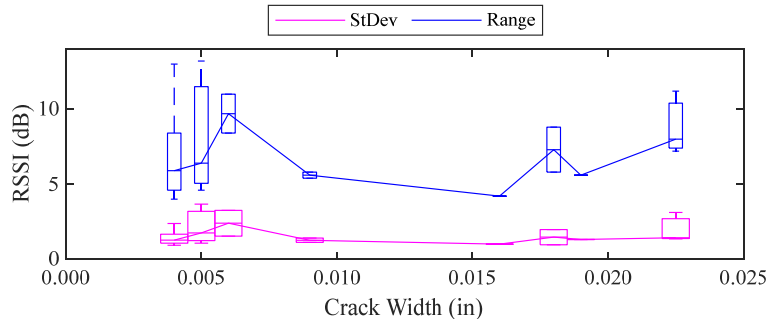Fig. 18 Correlation between average and mode RSSI and under crack width

Fig. 19 Correlation between standard deviation and range RSSI and under crack width

temperature does not have a significant influence on the StDev of the RSSI. The range of the RSSI changes between 5 dB and 10 dB, exhibiting outliers at higher temperatures.

Fig. 18 presents the average and mode of the RSSI relative to the temperature. The average and mode are reasonably aligned and shows a nonlinear anti-proportional relationship between the crack width by an average of 3 dB from 0.004 to 0.0225 inches.

Lastly, the StDev and range of the RSSI are plotted relative to crack width in Fig. 19. Similar to the StDev of the temperature, the StDev of the RSSI remained around 1 dB. However, the range of the RSSI does not show significant outliers throughout different categories of the crack widths.

The correlation of the average and mode of the RSSI, relative to temperature (Fig. 16) and to crack width (Fig. 18), showed similar results to one of testbed 1. Therefore, the damage identification method using ANN is employed for crack prediction as well.

5.2.3 Machine learning-based measures

Using the statistical measures and environmental conditions, an ANN data frame was created. This data frame contained average, mode, standard deviation, and range of raw RSSI values along with the temperature and crack width corresponding to the time and location of testing. This procedure, the identical procedure described in Figs. 2 and 3, and an MLR prediction method was employed for comparison. Both MLR and ANN models were trained using 90% of the data and the remaining 10% of data were used for crack prediction.

The process of training ANN for testbed 2 was identical to testbed 1. The loss function was plotted using a mean absolute error, Eq. (5), and a metric for model performance was used as the

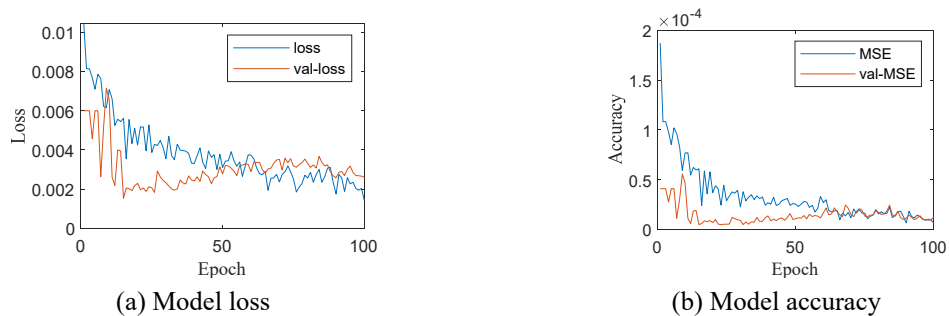

(a) Model loss   (b) Model accuracy

Fig. 20 Results for 90% trained ANN model

mean squared error, Eq. (4). Fig. 20 shows the training data along with the validation sets. Once more, convergence of training and validation data is observed as the number of epochs increases. Therefore, the successful training of ANN is assumed.

The predictions and error in prediction from the MLR and the ANN can be seen in Figs. 21 and 22, respectively. The data used for prediction allowed for one prediction for a few cases. This is not enough to determine performance on the MLR and ANN models for this testbed. For cases "0.0225 in" and "0.018 in", both predictions were incorrect by roughly 1%. Given the data used for prediction allowed for one prediction for a few cases, the increase of data would benefit the outcome of this prediction and therefore shows promise. For cases "0.006 in" and "0.004 in", the crack width was less than 0.01 inches. The model is expected to fail here due to the limitations presented by Sherpa *et al*. (2021). The sparse and small amount of experimental data caused the MLR to falsely conclude the negative crack prediction that correlation of the independent and dependent variables led to causation. Nonetheless, the ANN model prediction closely matched
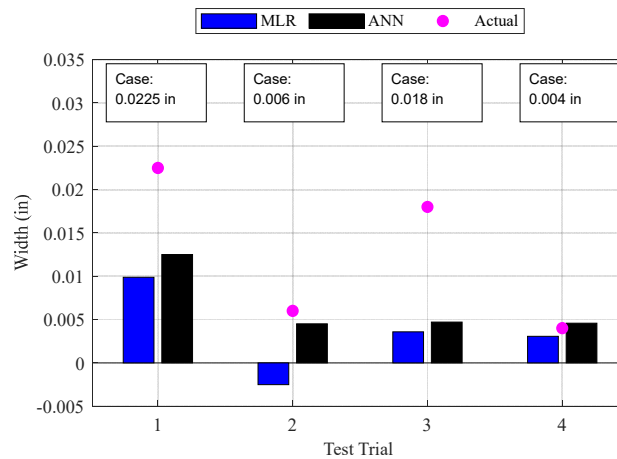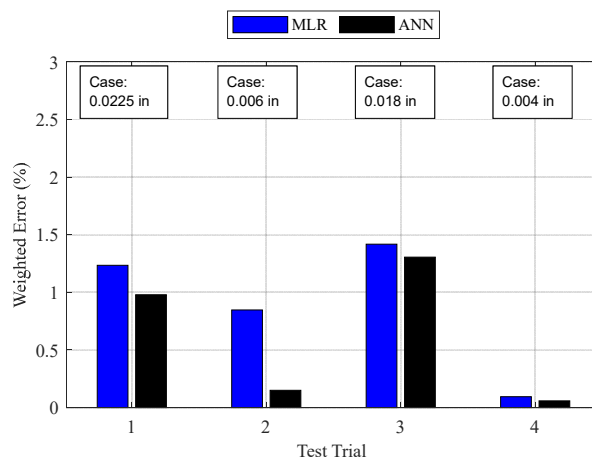

Fig. 21 Crack width predictions for MLR and ANN

Fig. 22 Error in crack width prediction from the MLR and ANN models

crack widths for "0.006 in" and "0.004 in" cases.

Using the weight error presented in Eq. (7) and the error in the model's prediction is presented in Fig. 22. The MLR had a 0.90% error with a standard deviation of 0.59% while the ANN had a 0.62% error with a standard deviation of 0.62%. For cases "0.006 in" and "0.004 in", the prediction error was 0.15% and 0.06% respectively, showing promise to experimental datasets that are sparse and small. Therefore, cracks of the residential building were successfully detected with the developed RFID-based sensing system with machine learning algorithms under temperature variability. Given the ANN and MLR models had 4 months of data instead of 12, the results show promise for future development. Other scopes of application for this cost-effective method of crack monitoring could be bridges as they often face cracking due to being greatly exposed to external forces. Additionally, bridges are greater used by the public and take in more traffic than buildings. This makes it more difficult to seal time and physical boundaries off to fix any severe cracking behavior that may occur. Based on this, several improvements can be made to the study design. More frequent testing would be ideal however this may be practically difficult as the testing site is a residential building. This would provide a more accurate picture as the changes are monitored day to day rather than month to month. Additionally, as it is difficult to distinguish between small changes in crack width within a fraction of 0.01 inches, a more accurate crack measurement method is needed for cracks smaller than 0.01 inches. With the current set-up, this method can be useful if the cracks from the crumbling foundation are greater than 0.01 inches, which would cover Categories 2 and 3 Crumbling Foundation with low cost. Further refinement is desired for the application for current structures before it is applied to bridges.

6. Conclusions

This paper demonstrated a successful crack monitoring algorithm with a developed RFID-based sensing system using machine learning under temperature variations. The crack monitoring algorithm was validated on two physical building structures in the field including: (1) crack detection on a reinforced concrete parking garage structure and (2) a residential crumbling foundation. A categorization of RSSI verse temperature was obtained for field conditions under extreme temperature fluctuations. The average and mode RSSI value were in alignment for both test beds regardless of temperature and crack width correlation. This indicates the temperature effect were controlled using the stated MMs and that average and mode RSSI can be interchanged if a controlled environment is achieved. The ANN model outperformed the MLR model in both building structures due to ability to differentiate crack vs non-crack cases and robustness no small perturbations. Although there was nonlinear behavior at 61°F, the ANN predicted the crack width within reasonable range. Further investigation on additional environmental factors that can affect the RSSI in the field situation is still underway to improve the crack prediction accuracy. The insight presented in this paper showed great potential of the developed RFID-based crack sensors for field implementation on building structures subject to crumbling foundations.

Acknowledgments

research at the University of Connecticut. In addition, the authors acknowledge the generous support and access to their home with crumbling foundation from an anonymous resident in Coventry, CT, and arrangement with Connecticut Transportation Institute (Director: James Mahoney).

References

Amajama, J. (2016), "Impact of weather components on (UHF) radio signal", *Int. J. Res. General Sci.*, **4**(3), 481-494.

ASCE (2017), Report Card for America's Infrastructure; American Society of Civil Engineers; Reston, Washington, DC, USA. https://www.infrastructurereportcard.org/wp-content/uploads/2016/10/2017-Infrastructure-Report-Card.pdf

ATID (2017), All the Identification AT870N Guide for Customer; All the Identification, Seoul, Korea. https://channel.invengo.com/download/support/AT870N_WinCE_User-Guide-2017-05_Eng.pdf

AtlasRFIDstore (2019), Alien Short RFID White Wet Inlay, ALN-9662, Higgs; AtlasFRIDstore, Alabama, USA. http://www.atlasrfidstore.com/alien-short-rfid-white-wet-inlay-aln-9662-higgs-3/

Brownlee, J. (2018), *How to Choose Loss Functions When Training Deep Learning Neural Networks*; Machine Learning Mastery, San Juan, Puerto Rico. https://machinelearningmastery.com/how-to-choose-loss-functions-when-training-deep-learning-neural-networks/

Bruciati, B., Jang, S. and Fils, P. (2019), "RFID-based crack detection of ultra high-performance concrete retrofitted beams", *Sensors*, **19**(7), 1573. https://doi.org/10.3390/s19071573

Daniels, J. (2020), *Ground Penetrating Radar*; U.S. Environmental Protection Agency, Washington, DC, USA. https://clu-in.org/characterization/technologies/gpr.cfm

Dormehl, L. (2019), "What is an Artificial Neural Network? Here's Everything You Need to Know", In: *Digital Trends*, Bristol, UK. https://www.digitaltrends.com/cool-tech/what-is-an-artificial-neural-network/

Duchesne, J. and Fournier, B. (2013), "Deterioration of concrete by the oxidation of sulphide minerals in the aggregate", *J. Civil Eng. Architect.*, **7**(8), 922. https://doi.org/10.17265/1934-7359/2013.08.003

Elshafey, A.A., Haddara, M.R. and Marzouk, H. (2010), "Damage detection in offshore structures using neural networks", *Marine Struct.*, **23**(1), 131-145. https://doi.org/10.1016/j.marstruc.2010.01.005

Federal Highway Administration (2001), Reliability of Visual Inspection for Highway Bridges: FHWA-RD-01-020. https://www.fhwa.dot.gov/publications/research/nde/pdfs/01020a.pdf

Fils, P.D. and Jang, S. (2020), "Wireless crack detection of a concrete building using low-cost RFID tags", In: *Sensors and Smart Structures Technologies for Civil, Mechanical, and Aerospace Systems*.

Giurgiutiu, V. and Craig, A.R. (1997), "Electro-mechanical (E/M) impedance method for structural health monitoring and non-destructive evaluation", *International Workshop on Structural Health Monitoring*, Stanford University, CA, USA, September.

Giurgiutiu, V. and Zagrai, A. (2005), "Damage detection in thin plates and aerospace structures with the electro-mechanical impedance method", *Struct. Health Monitor.*, **4**(2), 99-118. https://doi.org/10.1177/1475921705049752

Gobi, M. and Ashe, B. (2019), "Final Report of the Special Commission to Study the Financial and Economic Impacts of Crumbling Concrete Foundations due to the Presence of Pyrrhotite", Special Commission, The General Court, Commonwealth of Massachusetts.

Helwig, N.E. (2017), "Multivariate linear regression", University of Minnesota, Minneapolis and Saint Paul, MN, USA. http://users.stat.umn.edu/~helwig/notes/mvlr-Notes.pdf

Holleran, L. (2020), "Crumbling foundations", Connecticut State Department of Housing, Hartford, CT, USA. https://portal.ct.gov/DOH/DOH/Programs/Crumbling-Foundations

Kalansuriya, P., Bhattacharyya, R. and Sarma, S. (2013), "RFID tag antenna-based sensing for pervasive surface crack detection", *IEEE Sensors J.*, **13**(5), 1564-1570. https://doi.org/10.1109/jsen.2013.2240155

Keras (2015), *Keras documentation*: Losses; Mountain View, CA, USA. https://keras.io/api/losses/

Leonel, J. (2019), *Hyperparameters in Machine/Deep Learning*; Sao Paulo, Brazil.
https://medium.com/@jorgesleonel

Lienert, P. and Lee, J.L (2020), "Lidar laser-sensing technology: From self-driving cars to dance contests", Reuters, Las Vegas, NV, USA. https://www.reuters.com/article/us-tech-ces-lidar/lidar-laser-sensing-technology-from-self-driving-cars-to-dance-contests-idUSKBN1Z62AS

Marindra, A.M.J. and Tian, G.Y. (2019), "Multiresonance chipless RFID sensor tag for metal defect characterization using principal component analysis", *IEEE Sensors J.*, **19**(18), art. 8718341, 8037-8046. https://doi.org/10.1109/jsen.2019.2917840

Marindra, A.M.J., Sutthaweekul, R. and Tian, G.Y. (2018), "Depolarizing chipless RFID sensor tag for characterization of metal cracks based on dual resonance features", In: *International Conference on Information Technology and Electrical Engineering*: *Smart Technology for Better Society, ICITEE 2018*, 8534943, 73-78. https://doi.org/10.1109/iciteed.2018.8534943

Martínez-Castro, R.E., Jang, S., Nicholas, J. and Bansal, R. (2017), "Experimental assessment of an RFID-based crack sensor for steel structures", *Smart Mater. Struct.*, **26**(8), art. 085035. https://doi.org/10.1088/1361-665x/aa7cd8

Medeiros, R.D., Ribeiro, M.L. and Tita, V. (2014), "Computational methodology of damage detection on composite cylinders: structural health monitoring for automotive components", *Int. J. Automotive Compos.*, **1**(1), 112. https://doi.org/10.1504/IJAUTOC.2014.064159

Muller, M., Mitton, D., Talmant, M., Johnson, P. and Laugier, P. (2008), "Nonlinear ultrasound can detect accumulated damage in human bone", *Journal of Biomech.*, **41**(5), 1062-1068. https://doi.org/10.1016/j.jbiomech.2007.12.004

Park, G., Sohn, H., Farrar, C.R. and Inman, D.J. (2003), "Overview of piezoelectric impedance-based health monitoring and path forward", *Shock Vib. Digest*, **35**(6), 451-464.

Raju, V. (1998), "Impedance-based health monitoring technique of composite reinforced structure." *Proceedings of the 9th International Conference on Adaptive Structures and Technologies*, Cambridge, MA, USA, October. https://ci.nii.ac.jp/naid/10029700000

Ruder, S. (2017), An overview of gradient descent optimization algorithms; Dublin, Ireland. https://arxiv.org/pdf/1609.04747.pdf

Schaefer, B. and Schaefer, J. (2020), "Crumbling Foundations", Schaefer Inspection Service, Inc., Woodbridge, CT, USA. https://mhschaefer.com/crumblingfoundations-2/

Sepehry, N., Shamshirsaz, M. and Abdollahi, F. (2011), "Temperature variation effect compensation in impedance-based structural health monitoring using neural networks", *J. Intel. Mat. Syst. Str.*, **20**(10), 1-8. https://doi.org/10.1177/1045389X11421814

Sherpa, R., Fils, P. and Jang, S. (2021), "Crack detection of a reinforced concrete wall using low cost RFID-based sensors", *2021 Transportation Research Board Annual Meeting*, 1298 – Non-destructive Testing and Evaluation of Bridges, Washington DC, USA, January.

Sohn, H., Worden, K. and Farrar, C.R. (2002), "Statistical damage classification under changing environmental and operational conditions", *J. Intell. Mater. Syst. Struct.*, **13**(9), 561-574. https://doi.org/10.1106/104538902030904

Sun, F.P., Liang, C. and Rogers, C.A. (1994), "Structural modal analysis using collocated piezoelectric actuator/sensors: an electromechanical approach", In: *Smart Structures and Materials 1994*: *Smart Structures and Intelligent Systems*, Vol. 2190, pp. 238-249. https://doi.org/10.1117/12.175186

Unistress (1998), Unistress University of Connecticut Garage, Storrs, CT, USA. https://www.unistresscorp.com/portfolio/uconn/

Vitols Associates (2020), O&G; Torrington, CT, USA. https://www.ogind.com/portfolio/uconn-north-campus-parking-garage

Xia, Z.H. and Curtin, W.A. (2007), "Modeling of mechanical damage detection in CFRPs via electrical resistance", *Compos. Sci. Technol.*, **67**(7-8), 1518-1529. https://doi.org/10.1016/j.compscitech.2006.07.017

Xu, Y., Dong, L., Wang, H., Di, Y., Xie, X., Wang, P. and Zhang, M. (2019), "Reducing disturbance of crack location on crack depth-sensing tag", *Sensor Review*, **39**(4), 449-455.

https://doi.org/10.1108/sr-11-2018-0284

Xu, Y., Dong, L., Wang, H., Xie, X. and Wang, P. (2020), "Surface crack detection and monitoring in metal structure using RFID tag", *Sensor Review*, **40**(1), 81-88. https://doi.org/10.1108/sr-06-2019-0153

Zagrai, A.N. and Giurgiutiu, V. (2001), "Electro-Mechanical impedance method for crack detection in thin wall structures", In: *The 3rd International Workshop on Structural Health Monitoring*, Stanford University, CA, USA, September, pp. 77-86.

TY